Xu *et al.*
Journal of Analytical Science and Technology (2022) 13:41
https://doi.org/10.1186/s40543-022-00350-5

Journal of Analytical Science and Technology

RESEARCH ARTICLE Open Access

Development and validation of a new LC–MS/MS method for the determination of mefatinib in human plasma and its first application in pharmacokinetic studies

Yichao Xu, Jinliang Chen, Rong Shao, Zourong Ruan, Bo Jiang and Honggang Lou*

Abstract

Mefatinib (MET306) is a novel second-generation epidermal growth factor receptor-tyrosine kinase inhibitor (EGFR-TKI) designed to address the highly unmet clinical need of gefitinib-induced resistance and irreversibly bind to mutated tyrosine kinase domain of EGFR and human epidermal growth factor receptor 2 (HER2). In this study, a liquid chromatography–tandem mass spectrometry method was established and validated for determining MET306 in non-small cell lung cancer patients and a backpropagation artificial neural network was developed and constructed to predict the pharmacokinetic process. The mobile phase was water containing 5 mM ammonium acetate and acetonitrile at a flow rate of 0.3 mL min^{-1}, within a 4.5 min run time. MET306 was separated on a Hypersil Gold-C18 at 40 °C and subjected to mass analysis using positive electrospray ionization. A total of 524 data were used as development groups and 145 data were used as testing groups. The final established Northern Goshawk Optimization-Backpropagation Artificial Neural Network (NGO-BPANN) model consisted of one input layer with 6 neurons, 1 hidden layer with 10 nodes, and 1 output layer with one node processed by MATLAB2021a.The calibration range of MET306 was 0.5–200 ng mL^{-1} with the correlation coefficient $r \geq 0.99$. Accuracies ranged from 97.20 to 110.80% and the inter- and intra-assay precision were less than 15%. The ranges of extraction recoveries were 104.95% to 112.09% for analyte and internal standard and there was no significant matrix effect. The storage stability under different conditions was in accordance with the bioanalytical guidelines. The time-concentration profiles of the measured and predicted concentrations of MET306 by NGO-BPANN agree well. An NGO-BPANN model was developed to predict the plasma concentration and pharmacokinetic parameters of MET306 in the first time.

Keywords: MET306, LC–MS/MS, First in human, PK study, NGO-BPANN

Introduction

According to the latest research statistics, approximately 2.2 million people were diagnosed with cancer in 2020 worldwide, and 1.8 million people died of this disease. Approximately 11.4% of the diagnosed patients suffered from lung cancer, and 20% of cancer deaths were attributed to lung tumors (Sung et al. 2020). Non-small cell lung cancer (NSCLC) accounted for approximately 85% of lung malignant tumors, and most patients were diagnosed in the middle and late stages, with a 5-year survival rate of less than 20% (Pirlog et al. 2021; Wang et al. 2020; Dou and Jiang 2021). EGFR mutations are relatively common in NSCLC patients, and as many as 30–50% of patients in Asia are EGFR mutation-positive (Chan and Hughes 2015; Wang et al. 2016). Consequently, EGFR-TKI therapies have been developed, and the available studies show that these therapies are more

*Correspondence: louhg@zju.edu.cn

Center of Clinical Pharmacology, The Second Affiliated Hospital of Zhejiang University, School of Medicine, 88 Jiefang Road, Hangzhou 310009, Zhejiang, China

effective for the treatment of advanced lung cancer than recurrent chemotherapy or chemotherapy. Moreover, these therapies significantly improve patients' progression-free survival, as well as overall survival (Normando et al. 2015). The development of EGFR inhibitors completely revolutionized the treatment of NSCLC (Xu and Li 2021).

Gefitinib is the first EGFR-TKI approved for use in first-line treatment of metastatic NSCLC in 2016 (Takeda and Nakagawa 2019; Kitagawa et al. 2019). However, since its clinical application in 2003, studies have shown that approximately 50% of NSCLC patients will develop drug resistance after treatment with gefitinib for approximately 9–13 months (Arcila et al. 2011; Sharma et al. 2007). Secondary EGFR mutations, particularly T790M, are the most common mechanism of resistance acquired during EGFR-TKI treatment (Liu et al. 2017; Kobayashi et al. 2005).

MET306, a novel second-generation EGFR-TKI, was designed to overcome gefitinib-induced drug resistance by irreversibly binding to the mutated tyrosine kinase domain of EGFR and HER2. Unpublished preclinical studies reveal that the inhibitory activity of MET306 against mutant EGFR kinases is nearly 100 times higher than that of gefitinib, and that this EGFR-TKI has a very high inhibitory effect on gefitinib-resistant H1975 tumor cells. Moreover, preclinical pharmacokinetic studies show that MET306 is rapidly absorbed orally, with C_{max} attained after 2–4 h of administration. The bioavailability of MET306 in mice, rats, beagles, and monkeys is 45.2–100, 33.2–51.2, 66.3, and 10.5–27.9%, respectively. In addition, MET306 has a moderate plasma clearance, a large steady-state apparent volume of distribution, and a long half-life. In a recent study conducted on 106 patients with EGFR-mutant stage IIIB-IV NSCLC, it had been shown that the overall response rate (ORR) and disease control rate (DCR) corresponding to the group treated with daily doses of 60 ($n=51$) or 80 mg ($n=55$) MET306 are 84.9 and 97.25, respectively. The median progression-free survival (PFS) and overall survival (OS) are 15.4 and 31.6 months, respectively (Wang et al. 2021).

In this study, we establish a sensitive and reproducible LC–MS/MS method for the determination of MET306 concentration in the plasma. To the best of our knowledge, this concentration has never been reported in the literature before. The PK behavior of NSCLC patients administered with different doses of MET306 is also investigated. Moreover, the technology of machine learning, an artificial intelligence, was used to model and simulate the PK behavior of MET306 at different dose groups. A NGO-BPANN model was developed and validated to predict the plasma concentration of MET306 in NSCLC patients.

In general, the present study is an extension of our previous study, wherein we show that MET306 is an effective and well-tolerable first-line treatment of advanced EGFR-mutant NSCLC. The results reported herein will help provide patients with more precise and rational treatment options in the future.

Methods and materials

Chemicals and reagents

MET306 (purity: 99.49%) was bought from Jiangsu Ascentage Pharma Development Co., Ltd. (Jiangsu, China), whereas the internal standard MET306-d6 (purity: 92.8%) was obtained from Chengdu Chempartner Co., Ltd. (Chengdu, China). All the drug and IS were stored at − 20 °C before use. High-performance liquid chromatography (HPLC) grade methanol and acetonitrile were provided by Merck Company (Darmstadt, Germany), and ultrapure water was provided by a Millipore Direct-Q® ultrapure water system (Billerica, MA, USA). Blank human plasma was supplied by the Phase I Clinical Trials Unit at the Second Affiliated Hospital of Zhejiang University School of Medicine (Hangzhou, Zhejiang, China). All other chemicals were of analytical grade, and they were used without further purification.

Instruments

An LC-30AD liquid chromatograph (Shimadzu, Japan) coupled with an AB SCIEXQTRAP® 5500 tandem mass spectrometer (ABSCIEX, USA) and an HTC-xt PAL autosampler (CTC, Switzerland) was used for analysis. The samples were weighed and prepared using an XP-26 balance (Mettler-Toledo International Inc.) and an AllegraX-15R centrifuge (Beckman Coulter Inc.), respectively.

Analytical conditions

Chromatographic separation was achieved using a Hypersil Gold-C18 (2.1 mm × 50 mm, 1.9 μm) column kept at 40 °C and a mobile phase consisting of a mixture of 5 mM ammonium acetate solution (A) and acetonitrile (B). The flow rate of the mobile phase was set at 0.3 mL min^{-1}, and the gradient elution program was as follows: 0–0.5 min (5% B), 0.5–2 min (5–90% B), 0.2–3.5 min (90–90% B), and 3.51–4.5 min (5–5% B).

The AB SCIEXQTRAP® 5500 tandem mass spectrometer was operated in positive electrospray ionization (ESI) mode with multi-reaction monitoring (MRM), and the target ions for MET306 and the internal standard (IS) were m/z 466.2 → m/z 355.2 and m/z 472.2 → m/z 355.2, respectively. The flow rates of the Curtain Gas, Collision Gas, Ion Source Gas 1, and Ion Source Gas 2 were set at 40, 7, 20, and 60 L min^{-1}, respectively. The temperature was adjusted at 550 °C, and the ion spray voltage was 5000 eV.

Stock solutions and working solutions

The stock solutions of the analytes and IS were prepared in methanol, at the concentration of 1 mg mL^{-1} for each compound. The MET306 solution was serially diluted with methanol to prepare 10, 40, 100, 400, 800, 2000, and 4000 ng mL^{-1} standard working solutions of the analyte, whereas the IS solution was diluted to 8 ng mL^{-1}. The quality control working solutions of MET306 (3200, 320, 20, and 10 ng mL^{-1}) were also prepared by dilution in methanol. All standard and quality control working solutions were stored at − 20 °C before analysis. The calibration curve (0.5–200 ng mL^{-1}) and quality control samples of MET306 were prepared using blank plasma. The high- (HQC), medium- (MQC), and low-quality control (LQC) concentrations were 160, 16, and 1 ng mL^{-1}, respectively, whereas the lower limit of quantitation (LLOQ) was 0.5 ng mL^{-1}.

Sample extraction

MET306 was extracted from the plasma samples by protein precipitation. First, 50 μL of the collected plasma was pipetted into a 96-well plate along with 50 μL of the IS working solution (8 ng mL^{-1}), after thawing. Then, 200 μL of acetonitrile was added to the mixture, followed by vortex mixing at 1200 rpm for 2.0 min. Subsequently, the mixture was centrifuged at 3000×*g* for 10 min, and the collected supernatant (10 μL) was injected into the LC–MS/MS for analysis.

Validation parameters

The analytical method used herein was validated according to the 2013 FDA BMV guidelines and the 2016 ICH M10 BMV draft guideline. The Analyst®1.5.2 was used for data interpretation of LC–MS data. Specifically, the selectivity, lower limit of quantification, linearity, intra- and inter-batch precision, accuracy, carryover, extraction recovery, matrix effect, and stability were assessed.

Calibration curve and selectivity

The calibration curve was constructed by analyzing blank plasma samples spiked with the MET306 standard. Each sample was analyzed three times over at least two days. The peak area ratios of MET306 to IS were plotted against analyte concentrations to obtain the calibration curve that was used to determine the concentration of MET306 in the analytical plasma samples. The validity of the standard calibration curve in the range of 0.5–200 ng mL^{-1} was assessed based on linear regression, with a 1/x weighting factor.

Blank plasma samples were used to assess the selectivity of the analytical method at the LLOQ. The LLOQ value of MET306 was determined based on the precision (%CV) and accuracy criteria of 20% and ± 20% of the nominal concentration, respectively. The peak areas of interferents should not be more than 20% of the LLOQ peak area and 5% of the IS peak area.

Precision and accuracy

The precision and accuracy of the method were assessed by analyzing the 0.5, 1, 16, and 160 ng mL^{-1} quality control samples six times. Intra-day precision and accuracy were measured on the same day, whereas the inter-day values were determined based on three runs conducted over at least two days.

The accuracy calculated at each concentration level should be within ± 15% of the nominal concentration (LLOQ should be within ± 20%), while the precision (%CV) should not exceed 15% (LLOQ should not exceed 20%).

Carryover

Carryover investigations were performed by running six sequential analyses of blank samples and MET306 solutions at LLOQ (0.5 ng mL^{-1}) and ULOQ (200 ng mL^{-1}) concentrations. The carryover was considered to be acceptable if the peak area of MET306 in the blank sample was less than 20% of the peak area in the LLOQ, and the peak area of the IS in the blank sample was less than 5% of the original peak area.

Matrix effect and recovery

To verify the potential suppression or enhancement of ionization, the matrix effect was assessed by analyzing the blank matrices of six individual donors at the concentrations of 1 and 160 ng mL^{-1}. The matrix factors (MFs) of MET306 and IS were calculated as the ratios of the MET306 and IS peak areas detected in the presence of the matrix (measured by analyzing the blank plasma that had been spiked with the analyte after the extraction process) to those measured in the absence of it (pure solution), respectively. The IS-normalized MFs were obtained by dividing the MF values of MET306 by those of the IS. The CV % of the IS-normalized MFs corresponding to the six lots of matrices should be less than 15%.

The recovery of the method was determined by adding a known concentration of the analyte to the plasma before extraction and comparing the chromatographic peak areas of MET306 and IS in these samples to those obtained when the analyte was added after extraction. These analyses were repeated six times at each concentration (n = 6).

Stability

The stability of MET306 was evaluated by comparing the analyte peak areas of freshly prepared quality control

samples to those of plasma samples (1 and 160 ng mL^{-1} quality control concentrations) kept at different temperatures for varying periods (n = 3). Specifically, the samples analyzed were MET306-spiked samples kept at room temperature for 6 h, ready-to-inject samples (after protein precipitation) kept in the HPLC autosampler at 4 °C for 24 h, and samples stored at − 70 °C for 386 days. The first two sets of samples were used to assess short-term stability, whereas the last set was used to determine long-term stability. The stability of the stock solution of MET306 (1 mg mL^{-1}) and IS solution (8 ng mL^{-1}) was evaluated similarly, and the freeze/thaw stability was examined after four complete freeze/thaw cycles (− 70 to 37 °C) conducted on consecutive days.

PK study

The PK study was carried out between April 2016 and December 2017 at the Phase I Clinical Trials Unit of the Second Affiliated Hospital of Zhejiang University School of Medicine (Hangzhou, Zhejiang, China). The Good Clinical Practices and ethical principles enunciated in the amended Declaration of Helsinki (revised version of Fortaleza, 2013) were strictly followed. The protocols and amendments of this study were reviewed and approved by the Human Subject Research Ethics Committee of the Second Affiliated Hospital of Zhejiang University School of Medicine (Hangzhou, Zhejiang, China), and the study was registered at www.Chinadrugtrials.org.cn (CTR20160108 and CTR20160122).

The major inclusion criteria were as follows: (1) Willing to sign the informed consent; (2) age range from 18 to 75, regardless of gender; (3) histologically or cytologically confirmed NSCLC with stage IIIB to IV; (4) at any time since the initial diagnosis, there are clearly documented proven EGFR episodes associated with EGFR-TKI sensitivity Mutations; (5) the patient had at least one measurable lesion according to RECIST version 1.1, (6) ECOG strength score 0–1; (7) expected survival ≥ 3 months.

The major exclusion criteria were as follows: (1) The patient had been treated with EGFR-TKI; (2) patients received major surgery, chemoradiotherapy, immunotherapy, and other antitumor treatments that may interfere with the efficacy of the drug within 14 days before signing the informed consent; (3) patients who took adrenal steroid for more than two weeks in the first two weeks were screened; (4) pregnant or lactating women; (5) uncontrolled or active hepatitis B virus (HBV), hepatitis C virus (HCV) or HIV infection; (6) the researcher thinks it is not suitable to participate in this study.

The safety, tolerability, and pharmacokinetics of MET306 in patients with advanced NSCLC were assessed using a non-randomized, open-label, single, and multiple dosing escalation phase I clinical trial. In the first stage of this trial (single dosage stage), eligible patients were administered with a single dose of MET306 tablets and observed for 96 h before collecting the safety and tolerability data. In the second stage (multiple dosage stage), the patients were given an orally ingested tablet once a day for 14 consecutive days. In total, eight dosage groups of 10, 20, 30, 45, 60, 80, 105, 140 mg were investigated in this study.

Blood samples (2.5 mL each) were collected from each patient in K_2EDTA anticoagulant tubes before MET306 administration and at 1, 2, 3, 4, 5, 6, 8, 10, 12, 24, 48, 72, and 96 h after single dosing. In the multiple dosage stage, the samples were collected on days 17, 18, and 19 before the ingestion of the drug tablet, and on day 19, they were collected at 1, 2, 3, 4, 5, 6, 8, 10, 12, 24, 48, 72, and 96 h after ingestion. The blood samples were centrifuged at 3000 × *g* and 4 °C for 10 min, and after 60 min, the plasma-separated samples were stored at − 70 °C until analysis.

Metaheuristic optimization algorithms

Optimization algorithms are one of the efficient stochastic methods for solving optimization problems. In this study, the NGO algorithm is used, which simulates the behavior of the Northern Goshawk during prey hunting. This hunting strategy includes two stages of prey identification and tail-chasing processes (Dehghani et al. 2021).

The equation and parameter of initialization phase are as follows:

$$X = \begin{bmatrix} X_1 \\ \vdots \\ X_i \\ \vdots \\ X_N \end{bmatrix}_{N\times m} = \begin{bmatrix} X_{1,1} & \cdots & X_{1,j} & \cdots & X_{1,m} \\ \vdots & \ddots & \vdots & & \vdots \\ X_{i,1} & \cdots & X_{i,l} & \cdots & X_{i,m} \\ \vdots & & \vdots & \ddots & \vdots \\ X_{N,1} & \cdots & X_{N,j} & \cdots & X_{N,m} \end{bmatrix}_{N\times m}$$

$$F = \begin{bmatrix} F_1 \\ \vdots \\ F_i \\ \vdots \\ F_N \end{bmatrix}_{N\times 1} = \begin{bmatrix} F(X_1) \\ \vdots \\ F(X_i) \\ \vdots \\ F(X_N) \end{bmatrix}_{N\times 1}$$

$$X_{i,j} = l_j + rand \cdot \left(u_j - l_j\right), i = 1, 2, \ldots, N, j = 1, 2, \ldots, m$$

where X represents the entire population of pelicans, each X_i is a candidate solution to the given problem, and F stands for fitness function value. $X_{i,j}$ represents the value of the jth variable of the ith goshawk; N is the population size; m is the dimension; *rand* represents a random number between [0, 1]; l_j represents the lower limit; u_j represents the upper limit.

The equation and parameter of prey identification are as follows:

$$P_i = X_k, i = 1, 2, \ldots, N, k = 1, 2, \ldots, i-1, i+1, \ldots, N$$

$$x_{i,j}^{new,p_1} = \begin{cases} x_{i,j} + r\left(P_{i,j} - Ix_{i,j}\right), & F_{P_i} < F_i \\ x_{i,j} + r\left(x_{i,j} - P_{i,j}\right), & F_{P_i} \geq F_i \end{cases}$$

$$x_i = \begin{cases} x_i^{new,p_1}, & F_i^{new,p_1} < F_i \\ x_i, & F_i^{new,p_1} \geq F_i \end{cases}$$

where r is a random number belonging to [0,1]; I is a random number, which can be 1 or 2. When I=2, the displacement of each individual can be increased to make it enter a new area of the search space.

The equation of tail-chasing is as follows:

$$x_{i,j}^{new,p_2} = X_{i,j} + R(2r-1)X_{i,j}$$

$$R = 0.02\left(1 - \frac{t}{T}\right)$$

$$x_i = \begin{cases} x_i^{new,p_2}, & F_i^{new,p_2} < F_i \\ x_i, & F_i^{new,p_2} \geq F_i \end{cases}$$

BPANN modeling strategy

The BPANN is a machine learning technology that uses artificial intelligence systems to simulate the cognitive process of biological nerves to the outside world. The algorithm consists of forward transfer of information and back propagation of error (Grunert et al. 2013; Noorizadeh et al. 2013). The specific steps of BPANN are as follows: (a) use particle swarm algorithm to determine the initial weight and threshold of the model. (b) The input information is forwarded from the input layer through the hidden layer to the output layer and the output of each layer of neurons acts on the input of the next layer of neurons. c) If the output layer does not get the expected output, calculate the error change value of the output layer, propagate the error signal back along the original connection path through the network, and then modify the weights of each layer until the desired goal is achieved. The BPANN model can theoretically approximate any continuous function with arbitrary precision (Mei et al. 2019; Jun et al. 2020).

In this study, the groups of 10, 20, 30, 45, 60, 80 were used as development data to construct the NGO-BPANN model, and the groups of 105, 140 mg not involved in modeling were used as testing data to test the NGO-BPANN model.

Results

Calibration curve and selectivity

In the range of 0.5–200 ng mL^{-1}, the calibration curve of MET306 (variation of peak area ratio as a function of concentration) exhibits good linearity, with a regression coefficient ≥ 0.99. The equation of the linear fit is as follows: $y = (0.03926 \pm 0.002399)x + (0.002411 \pm 0.001928$), where x is the ratio of the MET306 peak area to that of IS, and y is the plasma concentration. The LLOQ concentration of MET306 in plasma samples is 0.5 ng mL^{-1}.

Figure 1 depicts the chemical structure and mass spectra of MET306 and IS. The LC–MS/MS chromatograms of these compounds are shown in Fig. 2. Notably, no interfering endogenous substances are observed at the retention times of MET306 and IS. The calibration curve figure is shown in Additional file 1: Fig S1. Clearly, no interfering endogenous substances are observed at the retention times of MET306 and the IS, implying acceptable selectivity.

Precision and accuracy

The measured concentrations of MET306 in each quality control sample (0.5, 1, 16, and 160 ng mL^{-1}) and the assay performance data of intra- and inter-day precision and accuracy are listed in Table 1. The CV% values of low-, medium-, and high-quality control samples are all less than 15%, and the value corresponding to the LLOQ sample is less than 20%. The accuracy of the method applied herein ranges between 97.20 and 110.80%.

Carryover

The amount of residual MET306 varies between 6.79 and 14.59% of the original concentration and is less than 20% of the LLOQ. Residual of IS is 0% of the LLOQ, which is obviously less than 5% of the LLOQ. Therefore, the results of autosampler carryover are acceptable.

Recovery and matrix effect

The results of recovery and matrix effect are presented in Table 1. The mean recoveries of MET306 at the concentrations of 1, 16, and 160 ng mL^{-1} are 113.19, 112.48, and 112.09%, respectively, and the recovery of IS is 92.25%.

The IS-normalized MFs of MET306 in 1 and 160 ng mL^{-1} quality control samples are found to be 1.02 and 1.01, and the CV% values corresponding to six lots of matrices at each concentration do not exceed 1.83%. Consequently, the matrix effect of the plasma is considered negligible.

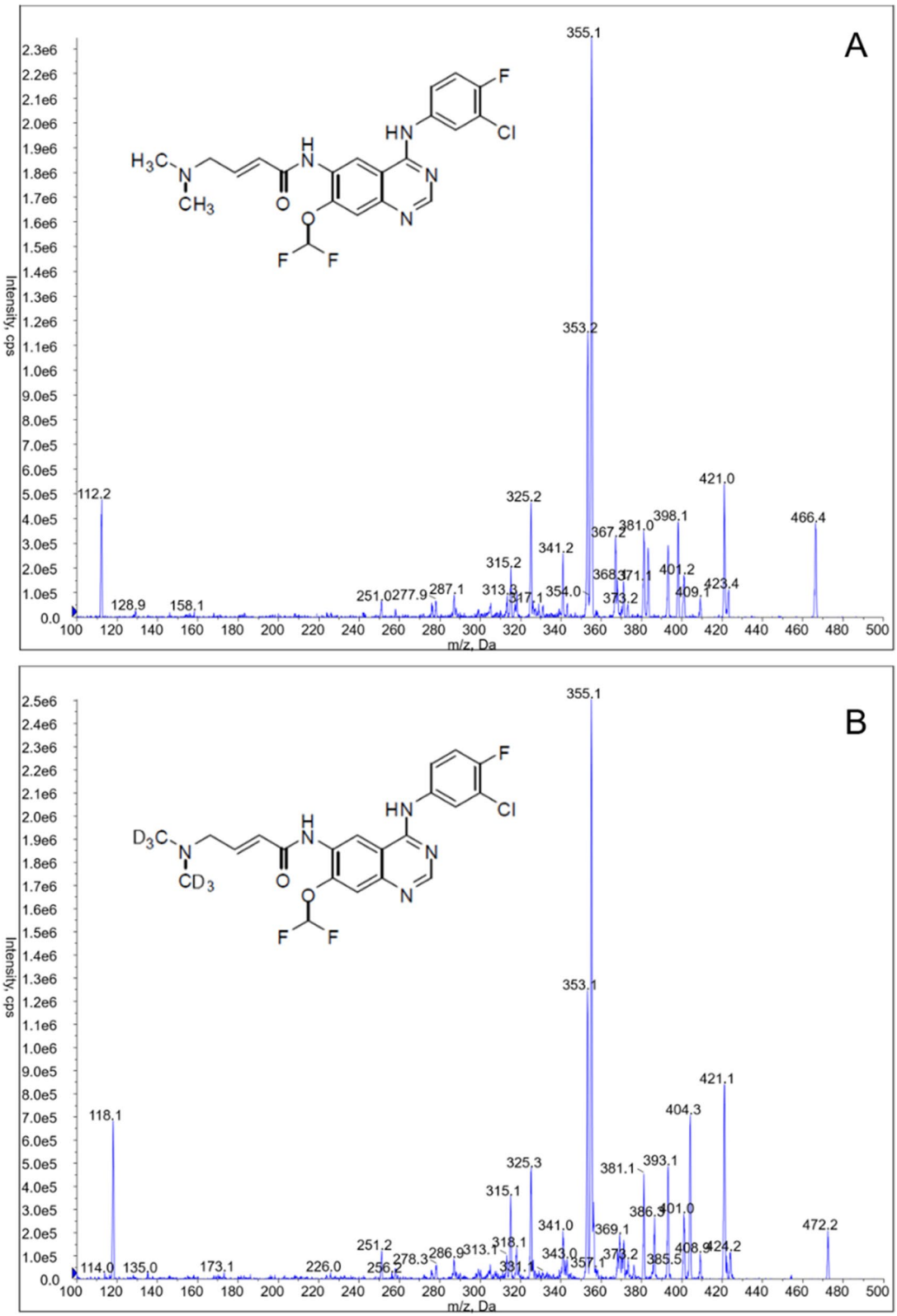

Fig. 1 The chemical structure and mass spectra of MET306 and IS. *The chemical structure and mass spectra of MET306 (**A**) and MET306-D_6 (**B**)

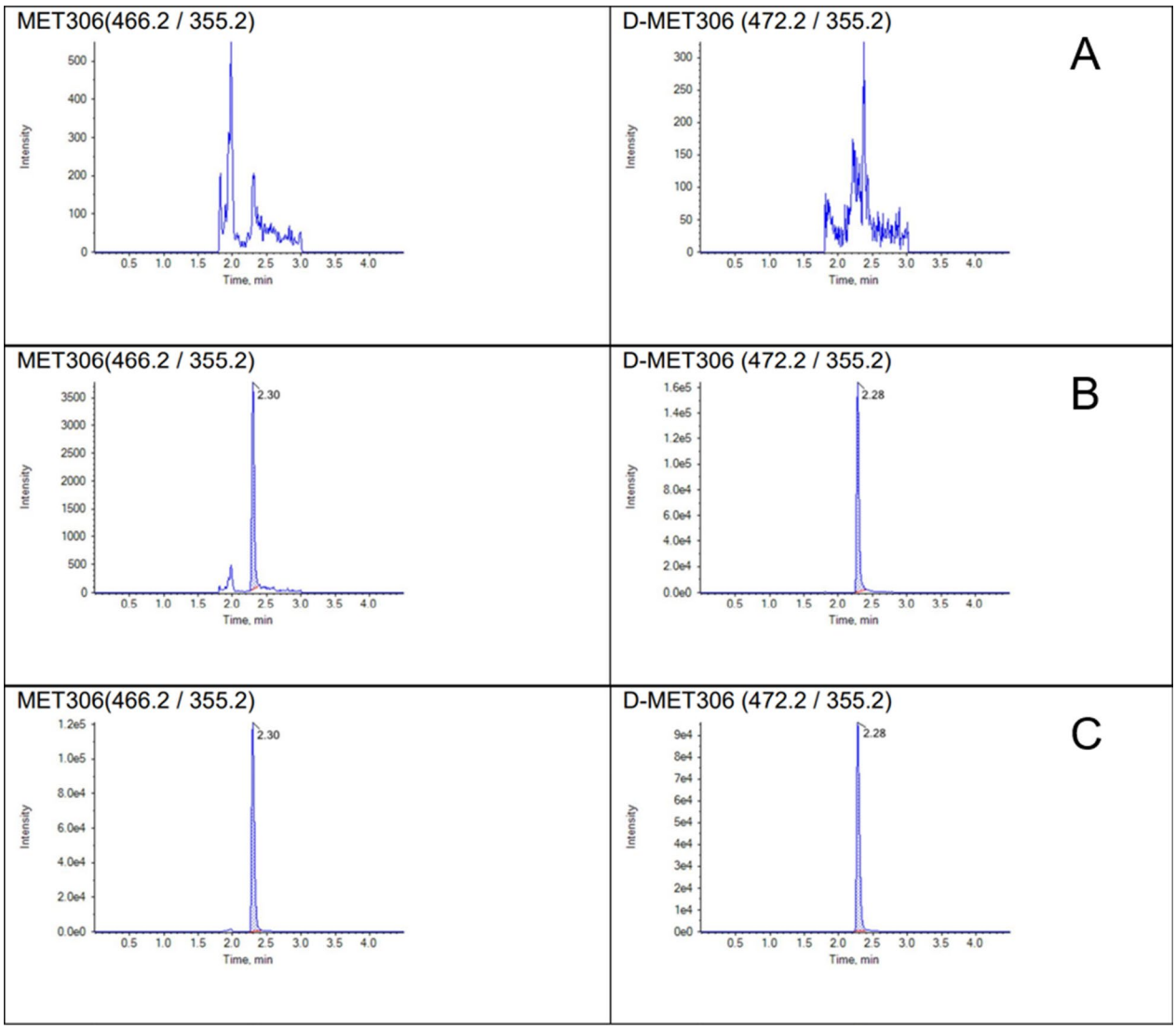

Fig. 2 Representative chromatograms of MET306 and IS in plasma. *The representative chromatograms of MET306 and IS in plasma: (**A**) a blank plasma sample; (**B**) LLOQ sample; (**C**) A plasma sample (3 h after dosing) of oral administration (30 mg) of MET306 in NSCLC patients

Stability

As shown in Table 2 and Additional file 1: Table S1, the short-term, long-term stability and dilution integrity of MET306 (6 h at room temperature, four freeze/thaw cycles, 24 h at 4 °C, 386 days at − 70 °C) and the stability of the stock solution of MET306 (1 mg mL^{-1}) and IS solution (8 ng mL^{-1}) are acceptable. In other words, MET306 is stable under a variety of storage conditions.

Pharmacokinetic study

The analytical method developed herein was used to determine the concentrations of MET306 in the plasma samples collected from NSCLC patients in different dose groups. The obtained results and main pharmacokinetic parameters determined using the non-compartmental method applied in the Phoenix Winnonlin 7.0 software (Certara, Princeton, NJ, USA) are summarized in Tables 3 and 4. The temporal evolution profiles of mean MET306 plasma concentration are shown in Figs. 3 and 4.

BPANN Modeling

A total of 524 data (19 patients, aged from 43 to 70) were used as development groups and 145 data (6 patients, aged from 45 to 69) were used as testing groups. The final established NGO-BPANN model consisted of one input layer with 6 neurons (dose, gender, stage, age, dosing data and dosing time), 1 hidden layer with 10 nodes, and 1 output

Table 1 Intra- and inter-day precision and accuracy, recovery and matrix effect of mefatinib in human plasma ($n = 6$)

Concentration (ng mL^{-1})	Intra-day			Inter-day			Recovery		Matrix effect	
	Mean ± SD (ng mL^{-1})	Accuracy (Bias %)	Precision (CV %)	Mean ± SD (ng mL^{-1})	Accuracy (Bias %)	Precision (CV %)	Mean ± SD	Precision (CV %)	Mean ± SD	Precision (CV %)
0.500 (LLOQ)	0.470 ± 0.0129	− 6.00	2.74	0.485 ± 0.0202	− 3.00	4.16	NA	NA	NA	NA
1.00 (LQC)	0.976 ± 0.0363	− 2.40	3.72	0.971 ± 0.0312	− 2.90	3.21	112.09 ± 2.20	1.96	1.02 ± 0.02	1.83
16.0 (MQC)	15.3 ± 0.297	− 4.38	1.94	15.2 ± 0.248	− 5.00	1.63	112.48 ± 2.50	2.22	NA	NA
160.0 (HQC)	157 ± 3.02	− 2.13	1.93	155 ± 2.68	− 3.13	1.73	113.19 ± 3.17	2.80	1.01 ± 0.01	1.33

Table 2 The stability of mefatinib in human plasma under a variety of storage and process conditions ($n = 6$)

Concentration (ng mL^{-1})	Short-term stability (room temp/6 h)		Long-term stability (− 70 °C/386 d)		Autosampler stability (4 °C/24 h)		Freeze–Thaw stability (4 cycles)		Dilution stability (dilution factor = 3)	
	Mean ± SD (ng mL^{-1})	CV (%)	Mean ± SD (ng mL^{-1})	CV (%)	Mean ± SD (ng mL^{-1})	CV (%)	Mean ± SD (ng mL^{-1})	CV (%)	Mean ± SD (ng mL^{-1})	CV (%)
1.00 (LQC)	0.988 ± 0.0340	3.46	0.985 ± 0.0960	9.72	1.01 ± 0.0451	4.46	0.997 ± 0.00234	0.23	NA	NA
160 (HQC)	155 ± 0.624	1.25	161 ± 5.40	3.36	156 ± 0.416	0.27	142 ± 2.76	1.94	NA	NA
300 (Dil-QC)	NA	NA	NA	NA	NA	NA	NA	NA	296 ± 3.19	1.08

Table 3 The main PK parameters in NSCLC patients after a single oral dose of MET306 tablets at different doses

Dose group (mg)	*n*	C_{max} (ng mL^{-1})	T_{max} (h)	$T_{1/2}$ (h)	AUC_{0-t} (ng h mL^{-1})	$AUC_{0-\infty}$ (ng h mL^{-1})	VD/F (L)	CL/F (L h^{-1})
10	1	14.6	5	21.8	268	296	1062	33.8
20	3	24.4 ± 7.97	5.00 ± 0.00	20.9 ± 2.02	535 ± 228	564 ± 236	1181 ± 403	40.2 ± 17.5
30	3	30.2 ± 8.72	5.34 ± 0.00	20.8 ± 3.64	838 ± 509	891 ± 553	1251 ± 603	45.0 ± 29.3
45	3	49.2 ± 13.3	4.33 ± 1.53	21.7 ± 0.28	1181 ± 359	1229 ± 372	1211 ± 322	38.8 ± 10.7
60	4	58.0 ± 33.5	4.50 ± 2.39	25.9 ± 6.78	1327 ± 693	1452 ± 808	1856 ± 847	55.3 ± 37.3
80	4	95.6 ± 28.3	4.50 ± 1.73	22.2 ± 3.1	2142 ± 695	2249 ± 760	1218 ± 340	39.12 ± 14.62
105	5	144.3 ± 84.7	4.40 ± 2.51	20.40 ± 3.17	2994 ± 2040	3323 ± 1890	1192 ± 619	41.80 ± 25.11
140	1	131.1	3	19.63	2582	2662	1490	52.6

Table 4 The main PK parameters (Day 19) in NSCLC patients after a multiple oral dose of MET306 tablets at different doses

Dose group (mg)	*n*	C_{max} (ng mL^{-1})	T_{max} (h)	$T_{1/2}$ (h)	AUC_{0-t} (ng h mL^{-1})	$AUC_{0-\infty}$ (ng h mL^{-1})	VD/F (L)	CL/F (L h^{-1})
10	1	11	6	30.2	323	362	2586	59.4
20	3	37.6 ± 11.6	5.00 ± 0.00	29.6 ± 1.95	1116 ± 357	1242 ± 413	1561 ± 494	37.0 ± 13.4
30	3	62.5 ± 22.4	4.67 ± 1.53	30.3 ± 2.88	1850 ± 970	2083 ± 1120	1577 ± 670	37.1 ± 19.3
45	3	73.1 ± 19.5	3.67 ± 1.15	28.0 ± 1.96	2177 ± 329	2381 ± 327	1561 ± 355	38.4 ± 6.25
60	4	90.4 ± 43.9	3.67 ± 2.08	27.9 ± 3.00	2983 ± 1996	3308 ± 2281	1979 ± 990	51.3 ± 30.2
80	4	166.6 ± 57.9	4.33 ± 3.51	29.6 ± 1.8	4393 ± 1281	4916 ± 1536	1430 ± 247	33.8 ± 7.3
105	5	184.4 ± 78.1	4.66 ± 1.52	28.35 ± 2.00	4843 ± 2242	5327 ± 2504	1837 ± 857	45.7 ± 24.1
140	1	194.2	2.98	30.2	4740	5162	2052	50.8

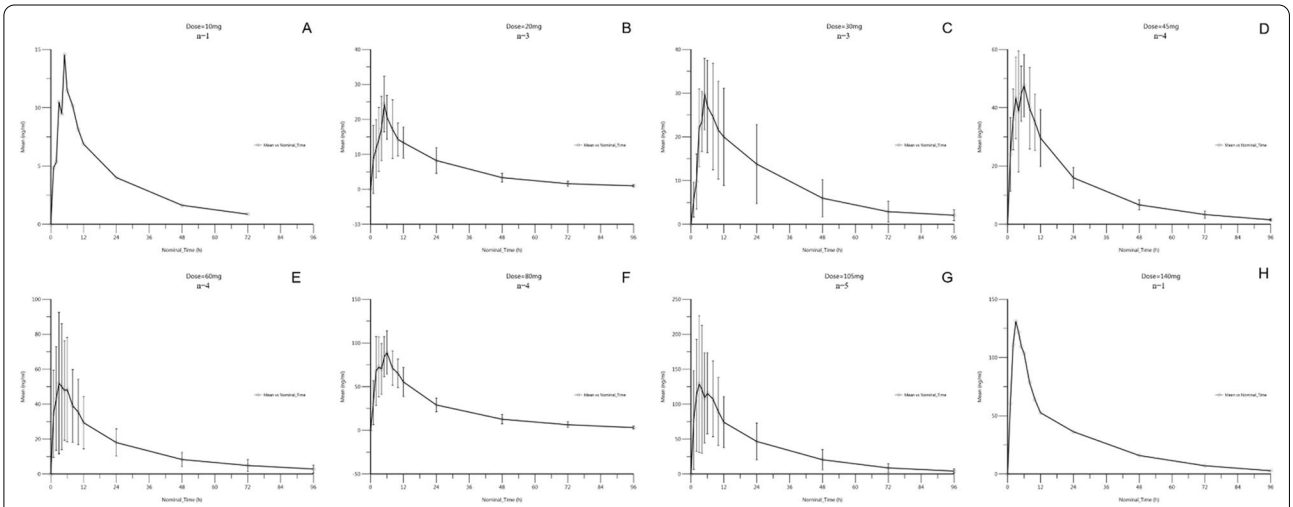

Fig. 3 The mean plasma concentration–time curves of NSCLC patients in different dose groups after single dosing of MET306. * The Mean ± SD plasma concentration–time profile of MET306 in human plasma following single oral administration of MET306 in different dose groups (**A**: 10 mg, **B**: 20 mg, **C**: 30 mg, **D**: 45 mg, **E**: 60 mg, **F**: 80 mg, **G**: 105 mg, **H**: 140 mg) to NSCLC patients (**A**: $n = 1$, **B**: $n = 3$, **C**: $n = 3$, **D**: $n = 4$, **E**: $n = 4$, **F**: $n = 4$, **G**: $n = 5$, **H**: $n = 1$)

layer with one node (plasma concentration of MET306) processed by MATLAB2021a. The basic structure schematic diagram is shown in Additional file 1: Fig. S2.

Many hyperparameters were used to train the net, where the number of training iterations was set to 100, the network performance target was 10^{-7}, and the learning rate was 0.1. The results indicated good performance: 0.00256 for MSE, 0.0163 for the magnitude of the gradient, and 6 for the number of validation checks. The Iterative curve of NGO-BPANN is shown in Fig. 5.

After the model was full validation, the data of groups of 105, 140 mg were used as testing data to test the NGO-BPANN model. The predicted and measured time-concentration profiles of MET306 in 105 and 140 mg groups are shown in Figs. 6 and 7, and the measured and predicted pharmacokinetic parameters are listed in Table 5.

Discussion

In this study, a simple (one-step protein precipitation) and sensitive (0.5 ng mL^{-1}) LC–MS/MS method with small sample volume (50 μL) and short run time (4.5 min) was developed to determine the concentration of MET306 in the plasma of NSCLC patients. The analytical method proposed herein was validated according to the guidelines of the 2013 FDA BMV and 2016 ICH M10 BMV drafts. The validation results show that the calibration curve linearity, selectivity, precision, accuracy, carryover, recovery, matrix effect, and stability criteria specified by these guidelines are all met. Notably,

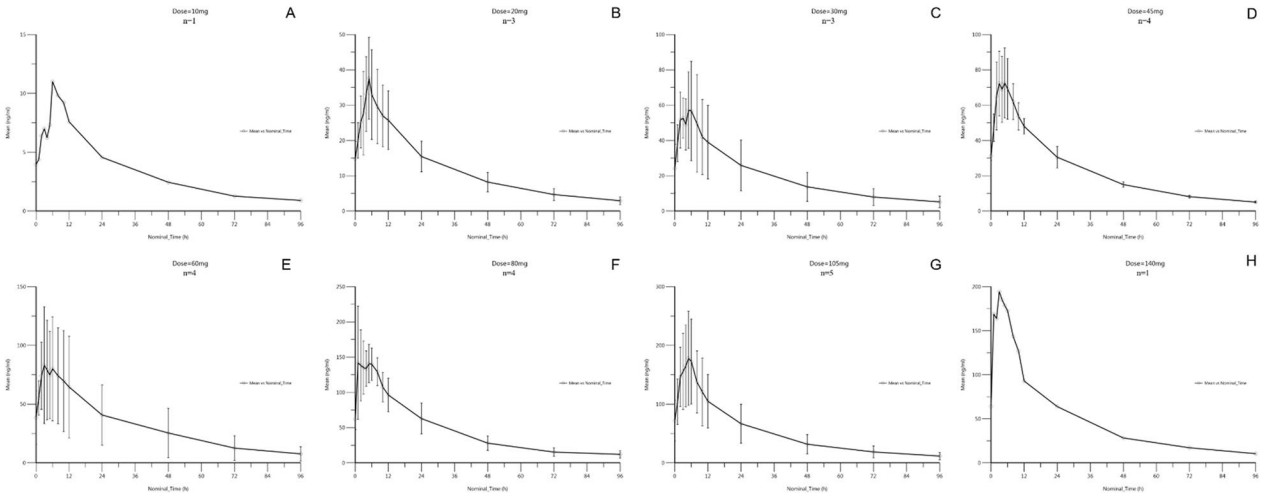

Fig. 4 The mean plasma concentration–time curves of NSCLC patients in different dose groups after multiple dosing of MET306. * The Mean ± SD plasma concentration–time profile of MET306 in human plasma following multiple oral administration of MET306 in different dose groups (**A**: 10 mg, **B**: 20 mg, **C**: 30 mg, **D**: 45 mg, **E**: 60 mg, **F**: 80 mg, **G**: 105 mg, **H**: 140 mg) to NSCLC patients (**A**: $n = 1$, **B**: $n = 3$, **C**: $n = 3$, **D**: $n = 4$, **E**: $n = 4$, **F**: $n = 4$, **G**: $n = 5$, **H**: $n = 1$)

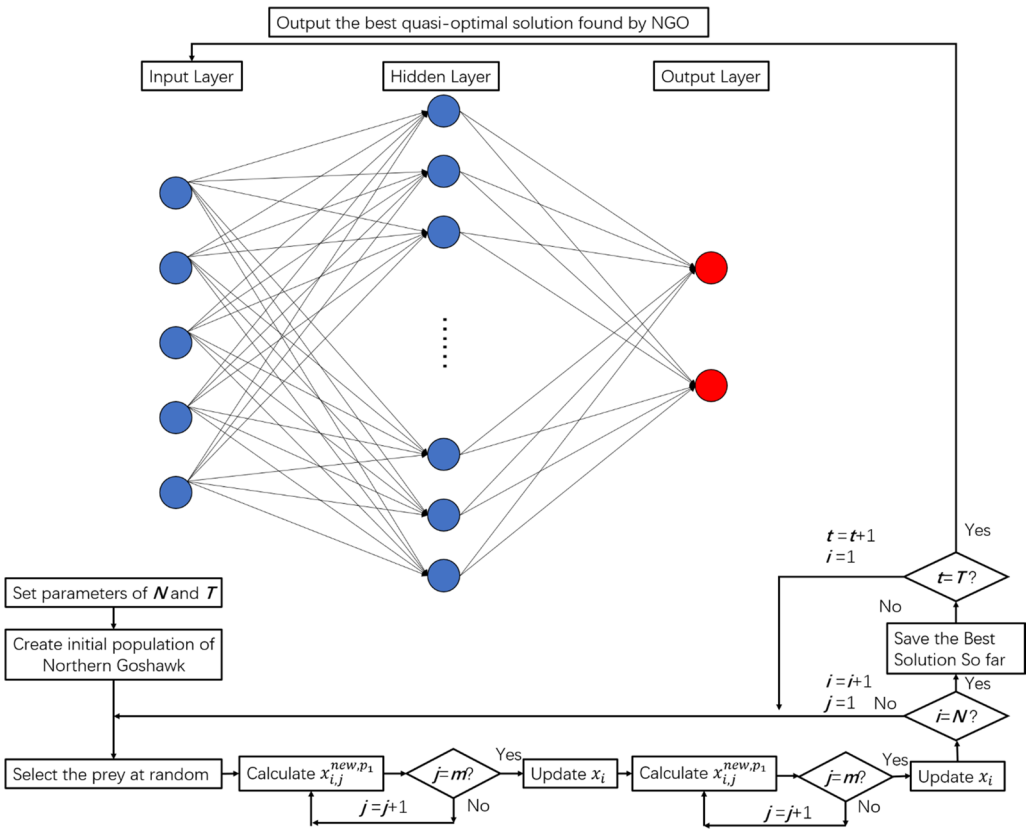

Fig. 5 The basic structure schematic diagram of Northern Goshawk Optimization-BPANN

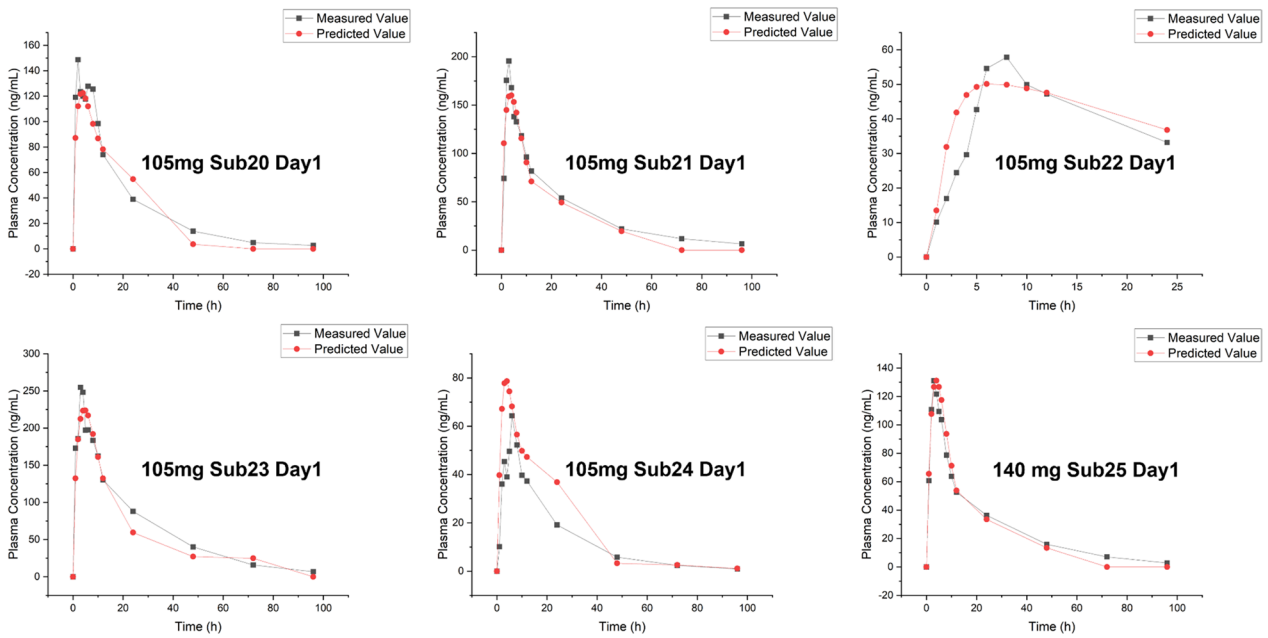

Fig. 6 The predicted and measured time-concentration profiles after single dosing of MET306 in 105 and 140 mg groups

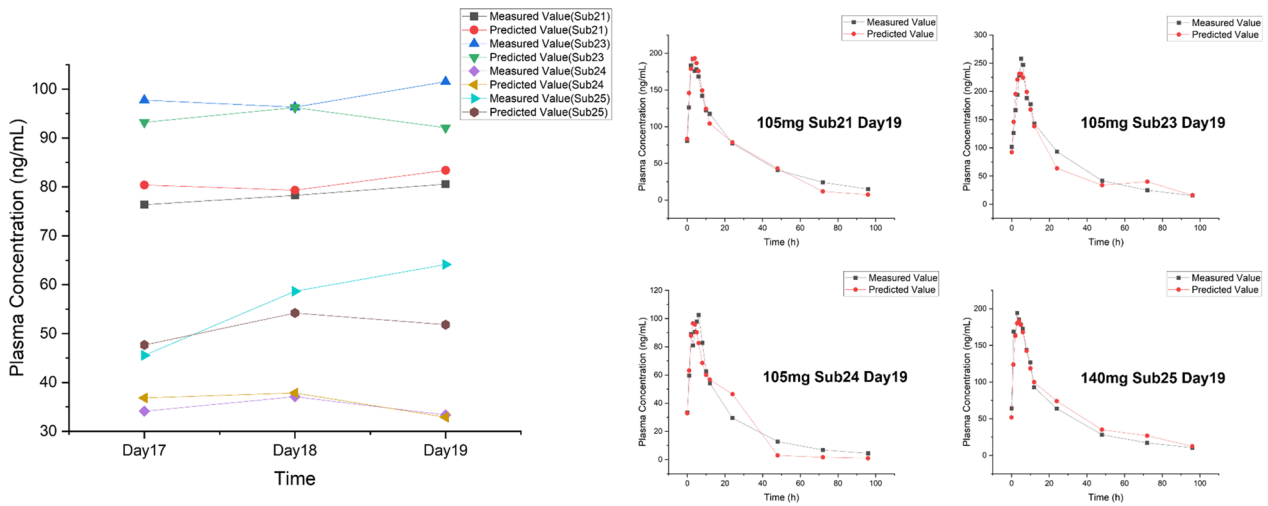

Fig. 7 The predicted and measured time-concentration profiles after multiple dosing of MET306 in 105 and 140 mg groups

the stability of MET306 at − 70 °C is as long as 386 days (LQC and HQC samples), which is suitable for the detection of this drug in clinical samples collected from NSCLC patients.

The method proposed in this study was used to detect the concentration of MET306 in the plasma of NSCLC patients administered with different doses of the drug. Based on the calculated PK parameters summarized in Tables 3 and 4, the main pharmacokinetic parameters (C_{max} and AUC_{0-t}) of the drug increase linearly of single dose MET306. Meanwhile, daily intake of MET306 for 14 days increases the AUC_{0-t} in NSCLC patients by 20–125%, depending on the dosage of the drug. This indicates that multiple oral administration of MET306 results in the accumulation of the drug in vivo.

BPANN was widely used during our pharmacokinetic research and plasma concentration prediction. In previous research, we predicted the plasma concentration and pharmacokinetic parameters of four bioequivalence studies of rosuvastatin calcium tablets (Xu et al. 2020),

Table 5 The measured and predicted main PK parameters in NSCLC patients after an oral dose of MET306 tablets at different doses

Administration	Dose group (mg)	Subject number	Measured value of C_{max} (ng mL^{-1})	Predicted value of C_{max} (ng mL^{-1})	Bias (%)	Measured value of AUC_{0-t} (ng h mL^{-1})	Predicted value of AUC_{0-t} (ng h mL^{-1})	Bias (%)
Single dose	105	20	148.8	122.4	− 17.72	2971	2721	− 8.41
	105	21	195.6	160.01	− 18.20	3811	3207	− 15.84
	105	22	57.87	50.13	− 13.37	949.6	1010	6.36
	105	23	254.8	223.79	− 12.17	5967	5256	− 11.91
	105	24	64.34	78.67	22.27	1275	1801	41.30
	140	25	131.1	131.1	0.02	2582	2363	− 8.48
Multiple dose	105	21	192.5	193.3	0.41	5628	5299	− 5.85
	105	23	258.1	231.2	− 10.43	6587	6217	− 5.61
	105	24	102.5	96.60	− 5.77	2314	2188	− 5.42
	140	25	194.2	183.3	− 5.63	4740	5297	11.75

predicted pharmacokinetics and the effect of genetic polymorphisms of deferasirox (Chen et al. 2020), and predicted the plasma concentration of febuxostat from different formulations (Xu et al. 2021). To our knowledge, this is the first time that the artificial intelligence system and the technology of machine learning were used to explore the plasma concentrations and pharmacokinetics parameters of new drugs in dose escalation studies. In this study, the stuck at the local minimum of the BPANN and the variable selection introduced were significant challenges during the research process. The NGO was introduced into modeling and the final model NGO-BPANN became more reliable and stable. The results showed that in testing groups, the bias of C_{max} was between − 18.20% and 22.27%. Meanwhile, the bias of AUC_{0-t} was between − 15.84% and 41.30% and the time–concentration profiles of the measured and predicted concentrations of MET306 by NGO-BPANN in 105 mg and 140 mg groups agree well. Thus, it is a promising tool to more precisely understand of pharmacokinetic process of MET306 in NSCLC patients.

Although the NGO-BPANN model developed in this study can successfully predict the pharmacokinetics of MET306, it has a few limitations. Firstly, this model is based on PK study of single and multiple administration of MET306, and it is validated in NSCLC patients with normal liver function and kidney function. However, it is not validated in patients with hepatic and renal insufficiency owing to the lack of clinical data. With the continuous development of MET306 study, NGO-BPANN model of special population will be further established. Secondly, there appears to be a difference in the plasma concentration and PK parameters in the 140 mg group; though the accuracy deviation was not large, the predicted results were lower than the measured ones during the multiple dosing phase. However, there was only one patient in the 140 mg group, we could not determine whether the prediction bias was due to randomness or nonlinearity PK of MET306 and we will explore this further in subsequent studies.

Conclusions

In this study, the presented LC–MS/MS method has been validated according to the FDA and ICH (US Department of Health and Human Services 2013; ICH 2016) guidance on bioanalytical method validation and is a simple, rapid and robust determination method for the quantification of MET306 in human plasma. It has been successfully applied to determine plasma concentrations of MET306 in samples from NSCLC patients. Moreover, an NGO-BPANN model was developed to predict the plasma concentration and pharmacokinetic parameters of MET306 in the first time. This model will serve as a helpful tool for providing useful information on the association of MET306 with toxicity and efficacy in NSCLC patient.

Supplementary Information

The online version contains supplementary material available at https://doi.org/10.1186/s40543-022-00350-5.

Additional file 1: The supplementary document of method validation and modeling.

Acknowledgements

The authors would like to thank the participating subjects and to acknowledge all clinical center personnel who contributed to this study. We thank LetPub (www.letpub.com) for its linguistic assistance during the preparation of this manuscript.

Author contributions

YX is the first author of this article, responsible for designing experiments, processing data and writing this article. JC is the author of this article, responsible for checking the data, reviewing the paper, and proposing amendments. RS is responsible for collecting demographic data and laboratory results from the subjects. ZR, HL and BJ are responsible for assisting in constructing and validating the BPANN models. All authors read and approved the final manuscript.

Funding
This work was supported by the National Major Science and Technology projects of China (No.2020ZX09201022).

Availability of data and materials
The datasets generated and analyzed during the current study are available from the corresponding author on reasonable request.

Declarations

Competing interests
All authors declare no competing interests for this work.

Received: 22 September 2022 Accepted: 31 October 2022
Published online: 14 November 2022

References

Arcila ME, Oxnard GR, Nafa K, Riely GJ, Solomon SB, Zakowski MF, Kris MG, Pao W, Miller VA, Ladanyi M. Rebiopsy of lung cancer patients with acquired resistance to EGFR inhibitors and enhanced detection of the T790M mutation using a locked nucleic acid-based assay. Clin Cancer Res. 2011;17:1169–80.
Chan BA, Hughes BG. Targeted therapy for non-small cell lung cancer: current standards and the promise of the future. Transl Lung Cancer Res. 2015;4:36–54.
Chen J, Xu Y, Lou H, Jiang B, Shao R, Yang D, Hu Y, Ruan Z. Effect of genetic polymorphisms on the pharmacokinetics of deferasirox in healthy Chinese subjects and an artificial neural networks model for pharmacokinetic prediction. Eur J Drug Metab Pharmacokinet. 2020;45:761–70.
Dehghani M, Hubálovský Š, Trojovský PJIA. Northern Goshawk optimization: a new swarm-based algorithm for solving optimization problems. IEEE Access. 2021;9:162059–80.
Dou Y, Jiang D. Research progress of small molecule anti-angiogenic drugs in non-small cell lung cancer. Chin J Lung Cancer. 2021;24:56–62.
Grunert T, Wenning M, Barbagelata MS, Fricker M, Sordelli DO, Buzzola FR, Ehling-Schulz M. Rapid and reliable identification of Staphylococcus aureus capsular serotypes by means of artificial neural network-assisted Fourier transform infrared spectroscopy. J Clin Microbiol. 2013;51:2261–6.
ICH M10. Final endorsed concept paper M10: bioanalytical method validation (2016). https://www.ich.org/fileadmin/Public_Web_Site/ICH_Products/Guidelines/Multidisciplinary/M10/ICH_M10_Concept_paper_final_7Oct2016.pdf.
Jun LY, Karri RR, Yon LS, Mubarak NM, Bing CH, Mohammad K, Jagadish P, Abdullah EC. Modeling and optimization by particle swarm embedded neural network for adsorption of methylene blue by jicama peroxidase immobilized on buckypaper/polyvinyl alcohol membrane. Environ Res. 2020;183:109158.
Kitagawa C, Mori M, Ichiki M, Sukoh N, Kada A, Saito AM, Ichinose Y. Gefitinib plus bevacizumab vs. gefitinib alone for EGFR mutant non-squamous non-small cell lung cancer. In Vivo (athens, Greece). 2019;33:477–82.
Kobayashi S, Boggon TJ, Dayaram T, Jänne PA, Kocher O, Meyerson M, Johnson BE, Eck MJ, Tenen DG, Halmos B. EGFR mutation and resistance of non-small-cell lung cancer to gefitinib. N Engl J Med. 2005;352:786–92.
Liu X, Wang P, Zhang C, Ma Z. Epidermal growth factor receptor (EGFR): a rising star in the era of precision medicine of lung cancer. Oncotarget. 2017;8:50209–20.
Mei Y, Yang J, Lu Y, Hao F, Xu D, Pan H, Wang J. BP-ANN model coupled with particle swarm optimization for the efficient prediction of 2-chlorophenol removal in an electro-oxidation system. Int J Environ Res Public Health. 2019;16:2454.
Noorizadeh H, Sobhan-Ardakani S, Raoofi F, Noorizadeh M, Mortazavi SS, Ahmadi T, Pournajafi K. Application of artificial neural network to predict the retention time of drug metabolites in two-dimensional liquid chromatography. Drug Test Anal. 2013;5:315–9.
Normando SR, Cruz FM, Del Giglio A. Cumulative meta-analysis of epidermal growth factor receptor-tyrosine kinase inhibitors as first-line therapy in metastatic non-small-cell lung cancer. Anticancer Drugs. 2015;26:995–1003.
Pirlog R, Cismaru A, Nutu A, Berindan-Neagoe I. Field cancerization in NSCLC: a new perspective on MicroRNAs in macrophage polarization. Int J Mol Sci. 2021;22:746.
Sharma SV, Bell DW, Settleman J, Haber DA. Epidermal growth factor receptor mutations in lung cancer. Nat Rev Cancer. 2007;7:169–81.
Sung H, Ferlay J, Siegel RL, Laversanne M, Soerjomataram I, Jemal A, Bray F. Global Cancer Statistics 2020: GLOBOCAN estimates of incidence and mortality worldwide for 36 cancers in 185 countries. CA Cancer J Clin. 2021;71:209–49.
Takeda M, Nakagawa K. First- and second-generation EGFR-TKIs are all replaced to osimertinib in chemo-naive EGFR mutation-positive non-small cell lung cancer? Int J Mol Sci. 2019;20:146.
US Department of Health and Human Services. Draft Guidance for Industry, Bioanalytical Method Validation. US FDA, Center for Drug Evaluation and Research, Center for Veterinary Medicine, MD, USA (2013).
Wang R, Chen C, Kang W, Meng GJAJOTR. SNHG9 was upregulated in NSCLC and associated with DDP-resistance and poor prognosis of NSCLC patients. Am J Transl Res. 2020;12:4456–66.
Wang P, Li Y, Lv D, Yang L, Ding L, Zhou J, Hong W, Chen Y, Zhang D, He S, Zhou J, Wang K. Mefatinib as first-line treatment of patients with advanced EGFR-mutant non-small-cell lung cancer: a phase Ib/II efficacy and biomarker study. Signal Transduct Target Ther. 2021;6:374.
Wang J, Wang B, Chu H, Yao Y. Intrinsic resistance to EGFR tyrosine kinase inhibitors in advanced non-small-cell lung cancer with activating EGFR mutations. Onco Targets Ther. 2016;9:3711–26.
Xu Y, Chen J, Yang D, Hu Y, Hu X, Jiang B, Ruan Z, Lou H. Development of LC–MS/MS determination method and backpropagation artificial neural networks pharmacokinetic model of febuxostat in healthy subjects. J Clin Pharm Ther. 2021;46:333–42.
Xu Z, Li J. Review on the combination strategy of anti-angiogenic agents and other anti-tumor agents in advanced non-small cell lung cancer. Chin J Lung Cancer. 2021;24:357–64.
Xu Y, Lou H, Chen J, Jiang B, Yang D, Hu Y, Ruan Z. Application of a backpropagation artificial neural network in predicting plasma concentration and pharmacokinetic parameters of oral single-dose rosuvastatin in healthy subjects. Clin Pharmacol Drug Dev. 2020;9:867–75.

Publisher's Note